

This is an Open Access document downloaded from ORCA, Cardiff University's institutional repository:<https://orca.cardiff.ac.uk/id/eprint/122822/>

This is the author's version of a work that was submitted to / accepted for publication.

Citation for final published version:

Scott, Alan F., Cresser-Brown, Joel, Williams, Thomas L., Rizkallah, Pierre J., Jin, Yi, Luk, Louis Y.-P. and Allemann, Rudolf K. 2019. Crystal structure and biophysical analysis of furfural detoxifying aldehyde reductase from clostridium beijerinckii. *Applied and Environmental Microbiology* 10.1128/AEM.00978-19

Publishers page: <http://dx.doi.org/10.1128/AEM.00978-19>

Please note:

Changes made as a result of publishing processes such as copy-editing, formatting and page numbers may not be reflected in this version. For the definitive version of this publication, please refer to the published source. You are advised to consult the publisher's version if you wish to cite this paper.

This version is being made available in accordance with publisher policies. See <http://orca.cf.ac.uk/policies.html> for usage policies. Copyright and moral rights for publications made available in ORCA are retained by the copyright holders.



1 Crystal Structure and Biophysical Analysis of Furfural Detoxifying Aldehyde Reductase from
2 *Clostridium beijerinckii*

3 Alan F. Scott^a, Joel Cresser-Brown^a, Thomas L. Williams^a, Pierre J. Rizkallah^b, Yi Jin^a, Louis Y.-
4 P. Luk^a, Rudolf K. Allemann^a#

5

6 ^aSchool of Chemistry, Cardiff University, Cardiff, United Kingdom

7 ^bInstitute of Infection & Immunology, School of Medicine, Cardiff University, Cardiff, U.K.

8 #Address correspondence to Rudolf K. Allemann: allemannrk@cardiff.ac.uk.

9 Running Head: Structure-function of a furfural reductase

10

11 Keywords:

12 lignocellulose, biofuel, detoxification, furfural tolerance, aldehyde reductase, isotope effects,

13 heavy enzyme, dynamic coupling

14 **Abstract**

15 Many aldehydes such as furfural are present in high quantities in lignocellulose lysates and are
16 fermentation inhibitors that make biofuel production from this abundant carbon source extremely
17 challenging. Cbei_3974 has recently been identified as an aldo-keto reductase responsible for
18 partial furfural resistance in *Clostridium beijerinckii*. Rational engineering of this enzyme could

19 enhance the furfural tolerance of this organism thereby improving biofuel yields. We report an
20 extensive characterization of Cbei_3974 and a single crystal X-ray structure of Cbei_3974 in
21 complex with NADPH at a resolution of 1.75 Å. Docking studies identified residues involved in
22 substrate binding and an activity screen revealed the substrate tolerance of the enzyme. Hydride
23 transfer, which is partially rate limiting under physiological conditions, occurs from the *pro-R*
24 hydrogen of NADPH. Enzyme isotope labeling revealed a temperature-independent enzyme
25 isotope effect of unity, indicating that the enzyme does not use dynamic coupling for catalysis
26 and suggests that the active site of the enzyme is optimally configured for catalysis with the
27 substrate tested.

28 **Importance**

29 Herein is reported the crystal structure and biophysical properties of an aldehyde reductase that
30 can detoxify furfural, a common inhibitor of biofuel fermentation found in lignocellulose lysates.
31 The data contained herein will serve as a guide for protein engineers to develop improved
32 enzyme variants that would infer furfural resistance to the microorganisms used in biofuel
33 production and thus lead to enhanced biofuel yields from this sustainable resource.

34

35 **Introduction**

36 An ideal source of carbohydrates for biofuel fermentation is lignocellulose, an abundant waste
37 product which is available at low cost and does not affect food security (1). Fermentable sugars
38 are most commonly released from lignocellulose using an acid pre-treatment (2). One of the
39 major drawbacks of this method is the release of aldehydes, organic acids and phenols, which
40 severely inhibit growth and limit the final yield of biofuel (3). While it has been observed that

41 *Clostridium* sp. has an increased tolerance against the aldehyde inhibitors, furfural and
42 hydroxymethylfurfural, when compared to other organisms, the high levels of inhibitors found in
43 lignocellulose lysates are nevertheless hugely problematic (4–6).

44 A recent investigation has identified two genes from *Clostridium beijerinckii* that encode
45 enzymes that reduce aldehydes to less toxic alcohols (7, 8). These enzymes showed activity
46 against furfural, hydroxymethyl furfural and benzaldehyde, which are all common fermentation
47 inhibitors (7). Furthermore, the genes encoding these enzymes are up-regulated during furfural
48 stress, suggesting the physiological relevance of these enzymes to protect *C. beijerinckii* (8). One
49 of these enzymes, Cbei_3904, belongs to the short chain dehydrogenase (SDR) family and the
50 other, Cbei_3974, to the aldo-keto reductase (AKR) family (7). It is highly desirable to engineer
51 greater catalytic efficiency into these enzymes to more rapidly eliminate toxic aldehydes thereby
52 enhancing resistance to aldehyde inhibition.

53 A prerequisite to rational engineering of an enzyme is a thorough understanding of its
54 mechanism. In this report, the furfural transforming AKR, Cbei_3974, is characterized to provide
55 valuable information for protein engineers. The substrate specificity, steady state kinetic
56 parameters and crystal structure of Cbei_3974 have been determined. In addition, the rate
57 limiting step of the reaction was identified and the coupling of dynamic motions to the active site
58 explored.

59

60 **Results**

61

62 **Substrate Profile.**

63 It has previously been suggested that Cbei_3974 may be useful to alleviate the toxicity of
64 furfural during the fermentation of acid treated lignocellulose lysates (7). NADPH dependent
65 activity towards furfural was previously reported for this enzyme but no characterization of the
66 reaction product was shown (7). To confirm that the enzyme indeed generates the less toxic
67 alcohol from the aldehyde, the reaction product from an enzyme-substrate-NADPH incubation
68 was analyzed by gas chromatography-mass spectrometry (GC-MS) in parallel with controls
69 containing no NADPH or no enzyme. After five hours incubation, a new compound can be
70 detected on the GC trace (Figure 1). The retention time and fragmentation pattern was identical
71 to a commercial standard of furfuryl alcohol. This compound was not detected in either of the
72 controls, showing that its formation was enzyme catalyzed and NADPH dependent.

73

74 Cbei_3974 has previously been shown to also exhibit activity with hydroxymethyl furfural,
75 benzaldehyde and butyraldehyde (7). To more fully explore the substrate scope of the enzyme, a
76 selection of aldehydes, ketones and alcohols were chosen. These putative substrates were
77 incubated at 2 mM with the enzyme and an excess of NADPH, NADH or NADP⁺. The change in
78 cofactor concentration was measured continuously by UV-spectroscopy to give the reaction rate
79 (Table 1). Surprisingly, L-glyceraldehyde-3-phosphate only gave negligible activity despite the
80 enzyme sharing 57.7 % identity with *Escherichia coli* YghZ, which converts L-glyceraldehyde-
81 3-phosphate to L-glycerol-3-phosphate as part of a novel triose phosphate isomerase (TIM)
82 bypass that allows the formation of dihydroxyacetone phosphate under gluconeogenic
83 conditions, when TIM is genetically inactivated (9). Purified YghZ was shown to reduce L-
84 glyceraldehyde-3-phosphate to L-glycerol-3-phosphate, which can be converted to
85 dihydroxyacetone by L-glycerol-3-phosphate dehydrogenase, thus complementing TIM

86 deficiency. Rather unexpectedly, YghZ is stereospecific for the *L*-enantiomer of the substrate,
87 whereas the TIM substrate is *D*-glyceraldehyde-3-phosphate. It was therefore proposed that a
88 spontaneous reaction may interconvert the two enantiomers (9). On this basis YghZ and
89 sequence similar enzymes, including Cbei_3974, are annotated in the KEGG database
90 (<https://www.kegg.jp/>) as *L*-glyceraldehyde-3-phosphate reductases (10, 11). Our results
91 demonstrate this annotation is incorrect for Cbei_3974.

92 Only minimal activity was found for the previously identified substrates, furfural and
93 butyraldehyde (7), while the enzyme had no measurable activity with benzaldehyde at the
94 concentrations tested (2 mM). In contrast, 4-pyridinecarboxaldehyde, which only differs from
95 benzaldehyde by the presence of a nitrogen atom in the aromatic ring, was the most kinetically
96 efficient among all of the substrates examined. Turnover was 17 times faster than for *L*-
97 glyceraldehyde-3-phosphate and 11 times faster than for furfural. Similarly, propionaldehyde did
98 not show activity at 2 mM while the more polar methylglyoxal, a dialdehyde of the same chain
99 length, gave strong activity 6.8 times faster than furfural. No activity could be detected with
100 ketones or alcohols at the concentrations tested.-The enzyme was specific for NADPH with no
101 activity detectable with 0.4 mM NADH. To determine whether the differences between
102 substrates was caused by differences in k_{cat} or K_M , steady state kinetics were measured for the 5
103 fastest substrates, not including 4-nitrobenzaldehyde, which was not soluble enough to achieve
104 saturation. All the aldehyde substrates resulted in Michaelis constants in the millimolar range but
105 NADPH had higher affinity as indicated by a lower K_M of 32 μ M (Table 2). The best substrate
106 was 4-pyridine carboxaldehyde with a k_{cat} of 10 s^{-1} and K_M of 3.87 mM. This was closely
107 followed by methylglyoxal with a similar k_{cat} of 8.52 s^{-1} but a higher K_M of 12.9 mM. Furfural
108 has previously been shown to have an extraordinarily high k_{cat} of $1.4 \times 10^5 s^{-1}$ at 40 °C (7). In our

109 experiments the k_{cat} was measured at 19 °C and was 2.72 s⁻¹. This was lower than expected, even
110 considering the lower temperature, but is more realistic. The K_M value of 34.9 mM measured
111 here is in agreement with the literature value (7).

112

113 **Stereochemistry of NADPH transfer**

114 The hydride transfer in aldehyde reductases occurs either from the *pro-R* or *pro-S* hydrogen on
115 C4 of the nicotinamide ring of NADPH. Typically, short-chain reductases (SDR) transfer the
116 *pro-S* hydrogen, while aldo-keto reductases (AKR) transfer the *pro-R* hydrogen (12). To
117 determine the stereospecificity of Cbei_3974, the enzyme was incubated with NADPH or (4*R*)
118 [4-²H]-NADPD with an excess of substrate 4-pyridinecarboxaldehyde. The reaction products
119 were analyzed to determine whether the deuterium had been incorporated into the alcohol
120 product or remained on the nicotinamide cofactor. The alcohol reaction product was extracted
121 with chloroform and analyzed by GC-MS. The incubation with (4*R*)-[4-²H]-NADPD gave a
122 product which was 1 atomic mass unit higher than the incubation with NADPH, consistent with
123 the incorporation of deuterium. In a duplicate reaction, the nucleotide product, NADP⁺, was
124 purified by ion exchange chromatography, freeze-dried and dissolved in D₂O. NMR analysis of
125 NADP⁺ from the reaction compared with commercial NADP⁺ showed identical spectra,
126 confirming that the deuterium at the *pro-R* position had been transferred from (4*R*)-[4-²H]-
127 NADPD (Figure 2). Cbei_3974 therefore transfers the *pro-R* hydrogen from NADPH in
128 accordance with other members of the AKR superfamily.

129

130 **Substrate Kinetic Isotope Effect (KIE).**

131 To ascertain if hydride transfer is the rate-limiting step, the substrate KIE for NADPH vs (4R)-
132 [4-²H]-NADPD was determined for a range of substrates. A KIE on k_{cat} of 2.13 - 2.58 was
133 observed across the 5 substrates tested (Figure 2) suggesting that the catalytic step is at least
134 partially rate limiting for all substrates tested.

135

136 **Heavy Enzyme Kinetic Isotope Effect.**

137 The effect of protein dynamics on catalysis was investigated by heavy enzyme production,
138 where the non-exchangeable carbon and nitrogen atoms were replaced with their heavy
139 counterparts (¹³C, ¹⁵N) to slow protein motions without affecting the electrostatics. A reactivity
140 difference between the “heavy” (labeled) and “light” (natural abundance) enzymes indicates that
141 protein motions impact on the catalysis (13). As the substrate KIE measurements indicated that
142 hydride transfer is partially rate limiting, steady-state measurements were used to determine any
143 effect that slower protein motions in heavy enzyme may have on the catalytic step.

144 Heavy enzyme (¹⁵N, ¹³C) was produced in M9 media with labeled feed-stocks and purified to
145 homogeneity (Figure S3). The incorporation of the heavy isotopes was confirmed by mass
146 spectrometry on the purified enzyme, which revealed a 5.5% mass increase (Figure S4). To
147 determine if the protein was correctly folded, the CD-spectrum and melting temperature were
148 recorded and compared for both the “heavy” and “light” enzymes (Figure S5). Both enzymes
149 gave identical spectra and largely identical melting temperatures of $62.4 \text{ }^{\circ}\text{C} \pm 0.1$ and $63.8 \text{ }^{\circ}\text{C} \pm$
150 0.2, respectively, indicating that isotopic labeling does not significantly alter protein folding.

151 Steady-state kinetics were used to determine k_{cat} for “heavy” and “light” enzyme with a range
152 of substrates at $19 \text{ }^{\circ}\text{C}$ (3). All substrates gave an enzyme KIE of near unity, implying that there
153 were no mass dependent effects and that dynamic coupling was minimal (Figure 3). Although

154 some authors have proposed that enzymes use “promoting motions” to drive catalysis (14–17),
155 this result is consistent with a growing body of literature that shows that dynamic effects only
156 become significant outside physiological conditions and only when poorly tolerated substrates
157 are utilized that necessitate rearrangement of the active site (18–20). The enzyme does not
158 therefore use dynamic motions as a part of its catalytic mechanism.

159 A recent study on the thermophilic alcohol dehydrogenase BsADH showed that significant heavy
160 enzyme KIEs only manifest below its physiological temperature (40 °C) and only with poor
161 substrates (19). The temperature dependency of heavy enzyme KIEs has been suggested to be an
162 indicator of whether an enzyme is optimized for utilization of a particular substrate (19). The
163 temperature dependence of the KIE for the Cbei_3974 catalyzed reduction of 3-pyridine
164 carboxaldehyde was constant over the temperature range from 11 to 44 °C (Figure 4) suggesting
165 that the active site architecture of the enzyme is optimized for this substrate.

166 **Single crystal X-ray Structure.**

167 The protein was co-crystallized with NADPH and the structure solved by molecular
168 replacement using PDB entry [5T79](#), which is the crystal structure for STM2406, an AKR from
169 *Salmonella typhimurium* of unknown physiological function but with a similar substrate profile
170 to Cbei_3974 (21). The two proteins have 60.91% sequence identity and a root mean square
171 deviation 0.89. The structure was refined at 1.75 Å to R_{factor} 16.5% (R_{free} 19.3%). The structure
172 consists of alternating α -helices and β -strands forming an 8 stranded TIM barrel with some extra
173 helices (Figure 5).

174 This motif is conserved across the AKR superfamily (23). Both this structure and STM2406
175 have an unusual N-terminus consisting of a long loop and a β -hairpin. Most AKR structures,
176 including the structure of *Coptotermes gestroi* AKR1 (another AKR known to reduce furfural),

177 have a shorter N-terminal tail consisting only of the β -hairpin or, in the case of the AKR7 family,
178 have no N-terminal tail (21, 24, 25). The function of this extra sequence is unclear. Conversely,
179 the C-terminus is truncated and is lacking a loop that is present in many AKRs, leaving the active
180 site exposed to solvent (25). AKRs, which omit this loop, have low catalytic efficiency
181 consistent with the measured millimolar Michaelis constants (21, 26, 27). Deletion of the C-
182 terminal loop from human aldose reductase AKR1B1 (27), *Bacillus subtilis* YhdN, YvgN and
183 *Pseudomonas aeruginosa* PA1127 (21) resulted in dramatic loss of catalytic efficiency.

184 NADPH sits in a mostly open cleft with a hydrophobic center and polar residues at the ends
185 where the adenine base and nicotinamide ring bind. The adenine base is held in place by
186 hydrogen bonds to Glu-307 and Asn-308. The nucleotide 2'-phosphate that distinguishes
187 NADPH from NADH, is hydrogen bonded to Gln-304 and Ser-300. The diphosphate makes
188 hydrogen bond contact with the backbone oxygen of Leu-225.

189 There is an area of missing electron density between residues Ile-238 to Leu-256. In
190 *Coptotermes gestroi* AKR1 and human aldose reductase, this region forms a mobile loop that
191 would strap the cofactor in place across the diphosphate bridge (24, 28). The lack of density in
192 Cbei_3974 indicates that the region is disordered and suggests that the loop is not trapping the
193 cofactor.

194 The canonical mechanism of AKRs involves hydride transfer from NADPH to the carbonyl
195 acceptor (12). This is followed by protonation from an active site tyrosine as part of a proton
196 relay from histidine and bulk water (12). Neighboring aspartate and lysine residues lower the p*K*_a
197 of tyrosine to enable it to function as an acid (12). In the close homologue STM2406, the
198 catalytic tetrad consists of Tyr-66, Asp-61, Lys-97 and His-138 (21). All these residues are
199 conserved in Cbei_3974 (identical numbering). It was not possible to obtain crystal structures of

200 protein-product complexes due to the low affinity of the ligands. Therefore, docking was used to
201 predict the possible binding of substrates. Autodock Vina (29) was used to dock furfural and the
202 best substrate, 4-pyridine carboxaldehyde, into the active site. The best pose was selected on the
203 basis of proximity to NADPH and the proposed catalytic residues. These poses are illustrated in
204 Figure 6. Both substrates are orientated towards the *pro-R* hydrogen of NADPH, consistent with
205 the experimentally determined stereochemistry. The carbonyl oxygen of 4-pyridine
206 carboxaldehyde is within hydrogen bonding distance of the exocyclic amide of NADPH and
207 makes hydrophobic contacts with residues Asn-65, Trp-33 and Tyr-100. These residues are
208 conserved in STM2406 and have been shown to be important for binding in that enzyme (21).
209 Furfural docked into the active site in a similar location but with a different orientation, possibly
210 due to its smaller size. The active site has a lot of polar residues, which may explain why the
211 more hydrophobic aldehydes such as benzaldehyde are less favored. Asn-65 and Tyr-100
212 contribute to the polar surface of the active site, and therefore alteration of these residues to more
213 hydrophobic ones may help improve activity for hydrophobic substrates. In STM2406, which has
214 a very similar active site, the variant Asn-65-Met (both enzymes have the same residue
215 numbering) gave 341% increase in activity towards 3-pyridinecarboxaldehyde, compared with
216 wild type and a 2-fold decrease in K_M (21). Alterations of Tyr-100 to aspartate, leucine,
217 isoleucine or valine mostly resulted in insoluble proteins, while Tyr-100-Ala showed decreased
218 activity but this may have been due to a loss of steric bulk by replacing a phenyl group with a
219 hydrogen atom (21).

220

221

222

223 **Discussion**

224 Cbei_3974, an enzyme that could putatively address the problem of aldehyde toxicity in
225 biofuel fermentation from lignocellulose (7), has been extensively characterized and its crystal
226 structure solved. Though annotated as an *L*-glyceraldehyde-3-phosphate reductase, it shows only
227 low activity towards this substrate. Instead, it preferentially catalyzes reactions with 4-pyridine
228 carboxaldehyde and methylglyoxal, of which only the latter is likely to be naturally occurring
229 inside the cell. Methylglyoxal is a toxic product formed from dihydroxy-acetone-phosphate by
230 methylglyoxal synthase to release phosphate (30). Detoxification of methylglyoxal by
231 *Clostridium* results in the formation of 1,2-propanediol in a pathway that requires aldo-keto
232 reductase activity (31). The physiological relevance of methylglyoxal reductase activity of
233 Cbei_3974 is however questionable, given the low affinity of the substrate with a K_M in the
234 region of 12 mM. The low affinity may be part of a mechanism to conserve NADPH, as
235 depletion of NADPH can be just as lethal as aldehyde accumulation (32) but this is unlikely
236 given the LD_{50} of methylglyoxal is likely to be significantly less than the K_M , rendering the
237 enzyme useless for detoxification. It is also possible that the enzyme requires an interaction
238 partner or a post-translational modification for activity or that the experimental conditions were
239 not optimal. An examination of the *C. beijerinckii* genome on the KEGG database (10, 11) shows
240 that the *cbei_3974* gene is not part of a biosynthetic gene cluster but it is adjacent to a putative
241 MerR transcription regulator. These typically respond to environmental stimuli to up-regulate
242 stress response proteins (33). In conclusion, the natural substrate of Cbei_3974 remains unclear
243 but it is likely to be involved in a stress response.

244 Studies with (4*R*)-[4-²H] NADPD demonstrated that hydride transfer occurs from the *pro-R*
245 hydrogen of NADPH and is partially rate limiting. Isotopically labeled heavy enzyme (¹³C, ¹⁵N)

246 gave identical k_{cat} constants to those obtained with the natural abundance enzyme, indicating that
247 the slower protein motions in the heavy enzyme did not impact the catalytic step. This shows that
248 the enzyme does not use “promoting motions” to drive the chemical transformation.

249 The enzyme kinetic isotope effect was independent of temperature suggesting that the
250 enzyme’s active site is optimally configured for the use of the tested substrates; the physiological
251 substrate is therefore likely to be structurally similar (19).

252 The crystal structure of Cbei_3974 revealed a typical AKR structure based around a TIM
253 barrel fold and is essentially the same as that of STM2406 (21). Docking of 4-
254 pyridinecarboxaldehyde and furfural revealed residues that may be involved in substrate binding.
255 Although no enzyme variants were generated in this study, these residues represent targets for
256 future work to generate an improved enzyme for more efficient detoxification of furfural.

257

258 **Materials and Methods**

259 **Material.**

260 A *pET-14b* vector harboring a codon optimized gene encoding Cbei_3974 was purchased from
261 GenScript (sequence in Figure S6). This also encodes a 6xHis tag and thrombin cleavage site
262 upstream of Cbei_3974.

263 NADPH was obtained from Fisher or Apollo Scientific. (4*R*)-[4-(2)H]NADPD was prepared
264 from NADP⁺ (Melford) and *d*₈ isopropanol (Acros) according to the published protocol (34).

265 ¹⁵N-NH₄Cl₂ and ¹³C-glucose were obtained from Goss Scientific, Cheshire, UK.

266 Furfural was obtained from VWR; methylglyoxal from Apollo Scientific; 3-pyridine
267 carboxaldehyde from Acros. All other chemicals were obtained from Sigma-Aldrich.

268

269 **Crystallography.**

270 Cbei_3974 was overproduced in BL21(DE3) cells and purified by Ni-affinity chromatography
271 as previously described (7). The protein was dialyzed against 10 mM HEPES-NaOH, pH 7.5,
272 300 mM NaCl and concentrated to 10 mg/mL. Crystallization trials were performed using the
273 sitting drop vapor diffusion method by mixing 0.5 µL protein stock solution and 0.5 µL of a seed
274 stock with 0.5 µL reservoir solution. The seed stock was obtained from microcrystals grown in
275 100 mM MOPS, pH 7.3, 13% PEG 8000, 750 mM NH₄Cl with 2 mM NADPH and 2 mM 4-
276 pyridine methanol. Diffracting crystals were obtained from 90 mM MOPS, pH 7.6, 271 mM
277 NH₄Cl, 2.7% PEG 8000, with 10 mM NADPH and 2 mM 4-pyridine methanol added to the
278 protein prior to crystallization. The crystals were transferred to cryoprotectant (90 mM MOPS,
279 pH 7.6, 271 mM NH₄Cl, 2.7% PEG 8000, 25% ethylene glycol) and flash-frozen with liquid
280 nitrogen.

281 The X-ray diffraction data was collected at 100K at Diamond Light Source (Oxfordshire,
282 U.K.) on Beamline I04-1 and integrated with XDS(35) in the xia2 package (36). The data were
283 scaled, reduced and analyzed with AIMLESS and TRUNCATE in the CCP4i (37). The structure
284 was solved by molecular replacement with PHASER (38) using coordinates from PDB 5T79 as
285 a searching model (21). The structure model was adjusted with COOT (39) and refined with
286 REFMAC5 (40). Graphical representations were prepared in Chimera(41), PyMOL (The
287 PyMOL Molecular Graphics System, Version 1.8.X Schrödinger, LLC), YASARA View(42)
288 and LigPlot+ (22).

289 **Accession Numbers.**

290 The X-ray structure solved in this study was deposited into the Protein Data Bank
291 (<http://www.rcsb.org/pdb/>), with accession code 6HG6.

292

293 **Molecular Docking.**

294 Ligand structures were downloaded from PubChem (<https://pubchem.ncbi.nlm.nih.gov/>) (43)
295 as SDF files and converted into mol2 format using Chimera (41). Ligand and protein were
296 converted into PDBQT format using AutoDockTools1.5.6 and docked using AutoDock Vina
297 (29). Graphical representations were prepared in PYMOL (The PyMOL Molecular Graphics
298 System, Version 1.8.X Schrödinger, LLC), Chimera (41), and LigPlot+ (22).

299

300 **Heavy and Natural Abundance Enzyme Production**

301 Arctic Express DE3 cells harboring *pET-14b_Cbei3974* were grown in 20 mL M9 minimal
302 medium containing 100 µg/mL carbenicillin overnight at 37 °C with shaking. This was diluted
303 1:50 into 0.5 L M9 media containing either natural abundance isotopes or ¹³C-glucose and ¹⁵N-
304 NH₄Cl₂ for heavy enzyme production. Cultures were grown to OD₆₀₀ 1.0 at 37 °C, 220 rpm.
305 Cultures were cooled to 12 °C and 0.4 mM IPTG was added to induce gene expression. Cells
306 were harvested at 4,000 rpm after 16 h growth at 12 °C, 200 rpm. The protein was purified as
307 previously described (7).

308

309 **Substrate Screen**

310 Cbei_3974 (0.585 µM), 0.4 mM NADPH, NADH or NADP⁺ and 2 mM putative substrate was
311 mixed in 20 mM K_iPO₄ pH 7.0. The subsequent change in NADPH concentration was monitored
312 at 340 nm ($e_{340} = 6220 \text{ M}^{-1} \text{ cm}^{-1}$) for 1 minute, using a Shimadzu UV-2401PC spectrophotometer
313 in 5 mm quartz cuvettes, to give the reaction rate.

314

315 **Enzyme Kinetics.**

316 Kinetic parameters were determined with 117 nM Cbei_3974 with one of the two substrates;
317 one held at saturating level while the other was varied across a concentration range of 0-75 mM
318 (aldehydes) or 0-0.2 mM (NADPH). Rates were measured as above and the data fitted to the
319 Michaelis-Menten equation using GraphPad Prism version 7.00 for Windows, GraphPad
320 Software, La Jolla California USA, www.graphpad.com. Each datapoint is the average of 3
321 repeats. For heavy enzyme kinetics, a minimum of two datasets of triplicates were collected.

322

323 **Mass Spectrometry.**

324 Liquid chromatography mass spectrometry (LC-MS) was performed on a Waters Synapt G2-Si
325 quadrupole time of flight mass spectrometer coupled to a Waters Acquity H-Class UPLC system.
326 The column was an Acquity UPLC protein BEH C4 (300 Å 1.7 µm x 2.1 mm x 100 mm)
327 operated in reverse phase and held at 60 °C. The gradient employed was 95% A to 35% A over
328 50 minutes, where A is H₂O with 0.1% HCO₂H and B is acetonitrile (ACN) with 0.1% HCO₂H.
329 Data was collected in positive ionisation mode and analyzed using the *Waters MassLynx*
330 software version 4.1. Deconvolution of protein charged states was obtained using the maximum
331 entropy 1 processing software.

332

333 **GC-MS analysis of reaction products.**

334 Mixtures containing 5 µM Cbei_3974, 4.6 mM NADPH or (4R)-[4-²H]-NADPD and 28 mM
335 aldehyde in a final volume of 40 µl 20 mM potassium phosphate pH 7.0 were incubated at 40 °C
336 for 1 hour. Aliquots (4 µL) were removed at time zero and at 5 or 7 hours and quenched with 1
337 ml of chloroform, which also served to extract the organic molecules. A 5 µl aliquot of the

338 organic layer was injected onto a PerkinElmer Clarus® 680 Gas Chromatograph. The initial
339 temperature was 40 °C, held for 1 minute and elution was with a gradient rising to 150 °C at 15
340 deg/min, holding at 150 °C for 1 minute. After a 3 minute solvent delay, mass spectra were
341 collected over the range 45 – 200 E+. Controls omitting either enzyme or NADPH were also
342 performed and a standard of furfuryl alcohol was run on the GC-MS.

343

344 **¹H NMR of Nicotinamide Cofactors.**

345 Cbei_3974 (1 mM), 2 mM (4*R*)-[4-²H]-NADPD and 25 mM 4-pyridine carboxaldehyde were
346 incubated at 37 °C for 3 hours. NADP⁺ was purified from the reaction on a SAX-10 column
347 using published methodology (34), freeze dried and re-dissolved in D₂O. Commercial standards
348 of NADPH and NADP⁺ were also dissolved in D₂O. NMR spectra of standards and reaction
349 product were collected on Bruker 400.

350

351 **Circular Dichroism.**

352 Circular dichroism (CD) measurements were performed on an Applied Photophysics Chirascan
353 spectrometer using 7 μM protein in 20 mM K_iPO₄ 20 % glycerol. Spectra was recorded over a
354 temperature range of 5 - 85 °C from 200 nm to 400 nm. The melting temperature was calculated
355 by fitting the data in SigmaPlot (Systat Software, San Jose, CA).

356

357 **Supporting Information.**

358 A PDF file with 6 pages containing: sequence of synthetic *cbei_3974* gene, SDS-PAGE
359 showing purity of proteins, mass spectrometry and circular dichroism of natural abundance and
360 heavy enzyme, and X-ray crystallography data collection and refinement statistics.

361 **Acknowledgements.**

362 We thank Diamond Light Source for access to beamline I04-1 (beamtime code mx1484-11).
363 Helpful discussions with Dr. Enas Behiry are gratefully acknowledged. This work was supported
364 by the UK's Biotechnology and Biological Sciences Research Council through grants
365 BB/J005266/1 and BB/L020394/1.

366

367 **References**

- 368 1. Isikgor FH, Becer CR. 2015. Lignocellulosic biomass: a sustainable platform for the
369 production of bio-based chemicals and polymers. *Polym Chem* 6:4497–4559.
- 370 2. Kumar P, Barrett DM, Delwiche MJ, Stroeve P. 2009. Methods for Pretreatment of
371 Lignocellulosic Biomass for Efficient Hydrolysis and Biofuel Production. *Ind Eng Chem
372 Res* 48:3713–3729.
- 373 3. Liu ZL, Blaschek HP. 2010. Biomass Conversion Inhibitors and In Situ Detoxification, p.
374 233–259. *In* Biomass to Biofuels. Blackwell Publishing Ltd., Oxford, UK.
- 375 4. Ezeji T, Qureshi N, Blaschek HP. 2007. Butanol production from agricultural residues:
376 Impact of degradation products on *Clostridium beijerinckii* growth and butanol
377 fermentation. *Biotechnol Bioeng* 97:1460–1469.
- 378 5. Zhang Y, Han B, Ezeji TC. 2012. Biotransformation of furfural and 5-hydroxymethyl
379 furfural (HMF) by *Clostridium acetobutylicum* ATCC 824 during butanol fermentation. *N
380 Biotechnol* 29:345–351.
- 381 6. Ujor V, Agu CV, Gopalan V, Ezeji TC. 2014. Glycerol supplementation of the growth

- 382 medium enhances in situ detoxification of furfural by Clostridium beijerinckii during
383 butanol fermentation. *Appl Microbiol Biotechnol* 98:6511–6521.
- 384 7. Zhang Y, Ujor V, Wick M, Ezeji TC. 2015. Identification, purification and
385 characterization of furfural transforming enzymes from Clostridium beijerinckii NCIMB
386 8052. *Anaerobe* 33:124–131.
- 387 8. Zhang Y, Ezeji TC. 2013. Transcriptional analysis of Clostridium beijerinckii NCIMB
388 8052 to elucidate role of furfural stress during acetone butanol ethanol fermentation.
389 *Biotechnol Biofuels* 6:66.
- 390 9. Desai KK, Miller BG. 2008. A Metabolic Bypass of the Triosephosphate Isomerase
391 Reaction. *Biochemistry* 47:7983–7985.
- 392 10. Kanehisa M, Sato Y, Kawashima M, Furumichi M, Tanabe M. 2016. KEGG as a
393 reference resource for gene and protein annotation. *Nucleic Acids Res* 44:D457–D462.
- 394 11. Kanehisa M, Furumichi M, Tanabe M, Sato Y, Morishima K. 2017. KEGG: new
395 perspectives on genomes, pathways, diseases and drugs. *Nucleic Acids Res* 45:D353–
396 D361.
- 397 12. Penning TM. 2015. The aldo-keto reductases (AKRs): Overview. *Chem Biol Interact*
398 234:236–46.
- 399 13. Kholodar SA, Ghosh AK, Kohen A. 2017. Measurement of Enzyme Isotope Effects.
400 *Methods Enzymol* 596:43–83.
- 401 14. Silva RG, Murkin AS, Schramm VL. 2011. Femtosecond dynamics coupled to chemical
402 barrier crossing in a Born-Oppenheimer enzyme. *Proc Natl Acadamy Sci U S A*

- 403 108:18661–18665.
- 404 15. Kipp DR, Silva RG, Schramm VL. 2011. Mass-dependent bond vibrational dynamics
405 influence catalysis by HIV-1 protease. *J Am Chem Soc* 133:19358–19361.
- 406 16. Pudney CR, Guerriero A, Baxter NJ, Johannissen LO, Waltho JP, Hay S, Scrutton NS.
407 2013. Fast Protein Motions Are Coupled to Enzyme H-Transfer Reactions. *J Am Chem
408 Soc* 135:2512–2517.
- 409 17. Antoniou D, Ge X, Schramm VL, Schwartz SD. 2012. Mass Modulation of Protein
410 Dynamics Associated with Barrier Crossing in Purine Nucleoside Phosphorylase. *J Phys
411 Chem Lett* 3:3538–3544.
- 412 18. Luk LYP, Loveridge EJ, Allemand RK. 2014. Different Dynamical Effects in Mesophilic
413 and Hyperthermophilic Dihydrofolate Reductases. *J Am Chem Soc* 136:6862.
- 414 19. Behiry E, Ruiz-Pernia JJ, Luk L, Tunon I, Moliner V, Allemand RK. 2018. Isotope
415 substitution of promiscuous alcohol dehydrogenase reveals origin of substrate preference
416 in transition state. *Angew Chem Int Ed* 57:3128–3131.
- 417 20. Ruiz-Pernía JJ, Behiry E, Luk LYP, Loveridge EJ, Tuñón I, Moliner V, Allemand RK.
418 2016. Minimization of dynamic effects in the evolution of dihydrofolate reductase. *Chem
419 Sci* 7:3248–3255.
- 420 21. Kim T, Flick R, Brunzelle J, Singer A, Evdokimova E, Brown G, Joo JC, Minasov GA,
421 Anderson WF, Mahadevan R, Savchenko A, Yakunin AF. 2017. Novel Aldo-Keto
422 Reductases for the Biocatalytic Conversion of 3-Hydroxybutanal to 1,3-Butanediol:
423 Structural and Biochemical Studies. *Appl Environ Microbiol* 83:e03172-16.

- 424 22. Laskowski RA, Swindells MB. 2011. LigPlot+: Multiple Ligand–Protein Interaction
425 Diagrams for Drug Discovery. *J Chem Inf Model* 51:2778–2786.
- 426 23. Sanli G, Dudley JI, Blaber M. 2003. Structural Biology of the Aldo-Keto Reductase
427 Family of Enzymes: Catalysis and Cofactor Binding. *Cell Biochem Biophys* 38:79–101.
- 428 24. Tramontina R, Franco Cairo JPL, Liberato M V., Mandelli F, Sousa A, Santos S, Rabelo
429 SC, Campos B, Ienczak J, Ruller R, Damásio ARL, Squina FM. 2017. The Coptotermes
430 gestroi aldo–keto reductase: a multipurpose enzyme for biorefinery applications.
431 *Biotechnol Biofuels* 10:4.
- 432 25. Barski OA, Tipparaju SM, Bhatnagar A. 2008. The aldo-keto reductase superfamily and
433 its role in drug metabolism and detoxification. *Drug Metab Rev* 40:553–624.
- 434 26. Ehrensberger AH, Wilson DK. 2004. Structural and Catalytic Diversity in the Two Family
435 11 Aldo-keto Reductases. *J Mol Biol* 337:661–673.
- 436 27. Bohren KM, Grimshaw CE, Gabbay KH. 1992. Catalytic effectiveness of human aldose
437 reductase. Critical role of C-terminal domain. *J Biol Chem* 267:20965–70.
- 438 28. Wilson DK, Bohren KM, Gabbay KH, Quiocho FA. 1992. An unlikely sugar substrate site
439 in the 1.65 Å structure of the human aldose reductase holoenzyme implicated in diabetic
440 complications. *Science* 257:81–4.
- 441 29. Trott O, Olson AJ. 2009. AutoDock Vina: Improving the speed and accuracy of docking
442 with a new scoring function, efficient optimization, and multithreading. *J Comput Chem*
443 31:NA-NA.
- 444 30. Huang K, Rudolph FB, Bennett GN. 1999. Characterization of methylglyoxal synthase

- 445 from Clostridium acetobutylicum ATCC 824 and its use in the formation of 1, 2-
446 propanediol. *Appl Environ Microbiol* 65:3244–7.
- 447 31. Liyanage H, Kashket S, Young M, Kashket ER. 2001. *Clostridium beijerinckii* and
448 *Clostridium difficile* Detoxify Methylglyoxal by a Novel Mechanism Involving Glycerol
449 Dehydrogenase. *Appl Environ Microbiol* 67:2004–2010.
- 450 32. Miller EN, Jarboe LR, Yomano LP, York SW, Shanmugam KT, Ingram LO. 2009.
451 Silencing of NADPH-dependent oxidoreductase genes (*yqhD* and *dkgA*) in furfural-
452 resistant ethanologenic *Escherichia coli*. *Appl Environ Microbiol* 75:4315–23.
- 453 33. Brown NL, Stoyanov J V, Kidd SP, Hobman JL. 2003. The MerR family of
454 transcriptional regulators. *FEMS Microbiol Rev* 27:145–63.
- 455 34. Loveridge EJ, Allemann RK. 2011. Effect of pH on Hydride Transfer by *Escherichia coli*
456 Dihydrofolate Reductase. *ChemBioChem* 12:1258–1262.
- 457 35. Kabsch W. 2010. XDS. *Acta Crystallogr D Biol Crystallogr* 66:125–32.
- 458 36. Winter G, IUCr. 2010. *xia2*: an expert system for macromolecular crystallography data
459 reduction. *J Appl Crystallogr* 43:186–190.
- 460 37. Winn MD, Ballard CC, Cowtan KD, Dodson EJ, Emsley P, Evans PR, Keegan RM,
461 Krissinel EB, Leslie AGW, McCoy A, McNicholas SJ, Murshudov GN, Pannu NS,
462 Potterton EA, Powell HR, Read RJ, Vagin A, Wilson KS. 2011. Overview of the CCP 4
463 suite and current developments. *Acta Crystallogr Sect D Biol Crystallogr* 67:235–242.
- 464 38. McCoy AJ, Grosse-Kunstleve RW, Adams PD, Winn MD, Storoni LC, Read RJ. 2007.
465 Phaser crystallographic software. *J Appl Crystallogr* 40:658–674.

- 466 39. Emsley P, Cowtan K. 2004. *Coot*: model-building tools for molecular graphics. *Acta*
467 *Crystallogr Sect D Biol Crystallogr* 60:2126–2132.
- 468 40. Murshudov GN, Vagin AA, Dodson EJ, IUCr. 1997. Refinement of Macromolecular
469 Structures by the Maximum-Likelihood Method. *Acta Crystallogr Sect D Biol Crystallogr*
470 53:240–255.
- 471 41. Pettersen EF, Goddard TD, Huang CC, Couch GS, Greenblatt DM, Meng EC, Ferrin TE.
472 2004. UCSF Chimera?A visualization system for exploratory research and analysis. *J*
473 *Comput Chem* 25:1605–1612.
- 474 42. Krieger E, Vriend G. 2014. YASARA View—molecular graphics for all devices—from
475 smartphones to workstations. *Bioinformatics* 30:2981–2982.
- 476 43. Kim S, Thiessen PA, Bolton EE, Chen J, Fu G, Gindulyte A, Han L, He J, He S,
477 Shoemaker BA, Wang J, Yu B, Zhang J, Bryant SH. 2016. PubChem Substance and
478 Compound databases. *Nucleic Acids Res* 44:D1202-13.

479 **TABLES:**

480 Table 1. Substrate Screen

481 Activity of Cbei_3974 with putative substrates (2 mM) and 0.4 mM NADPH. Errors indicate
482 standard deviation of three repeats. n.d. = no detectable activity

483

Substrate	Specific Activity $\mu\text{mols/min/mg}$
furfural	416.86 \pm 4.81
benzaldehyde	n.d.
4-pyridine carboxaldehyde	4,652.70 \pm 671.05
3-pyridine carboxaldehyde	1,519.52 \pm 61.48
4-nitrobenzaldehyde	4,390.44 \pm 61.61
isatin	n.d.
methylglyoxal	2,852.59 \pm 335.72
formaldehyde	n.d.
acetaldehyde	n.d.
propionaldehyde	n.d.
butyraldehyde	307.37 \pm 23.65

valeraldehyde	n.d.
furfural alcohol	n.d.
benzyl alcohol	n.d.
4-pyridine methanol	n.d.
methanol	n.d.
ethanol	n.d.
isopropyl alcohol	n.d.
butanol	n.d.
2,4-pentanedione	n.d.
4-acetylpyridine	n.d.
2-butanone	n.d.
<i>L</i> -arabinose	n.d.
<i>D</i> -glucose	n.d.
β -lactose	n.d.
<i>L</i> -glyceraldehyde-3-phosphate	269.71 ± 34.05

485 Table 2. Kinetic measurements for Cbei_3974.

486 All measurements at 19 °C. Errors show the standard error from fitting the data to the

487 Michaels-Menten equation in GraphPad Prism.

488

Substrate	$k_{\text{cat}} / \text{s}^{-1}$	K_M / mM	$k_{\text{cat}}/K_M \text{ s}^{-1} \text{ M}^{-1}$
furfural	2.72 ± 0.27	34.9 ± 7.6	78
butyraldehyde	5.16 ± 1.04	40.79 ± 4.5	127
3-pyridine carboxaldehyde	4.97 ± 1.38	15.7 ± 2.6	317
methylglyoxal	8.52 ± 0.26	12.9 ± 1.5	660
4-pyridine carboxaldehyde	10.60 ± 0.2	3.87 ± 0.34	2,739
NADPH (with 4-pyridine carboxaldehyde)	10.0 ± 1.02	0.032 ± 0.02	312,500
NADPH (with furfural)	2.59 ± 0.145	0.015 ± 0.003	172,666

489 **FIGURES:**

490

491 Figure 1. GC-MS analysis of the Cbei_3974 reaction product

492 (a) mixture of enzyme, NADPH and furfural at time zero, (b) incubation of furfural and
493 NADPH without enzyme after 5 hours, (c) incubation of furfural and enzyme without NADPH
494 for 5 hours, (d) incubation of furfural, NADPH and enzyme after 5 hours, (e) as d but doped with
495 furfuryl alcohol, (f) standard of furfuryl alcohol, (g) mass spectrum of reaction product from
496 incubation of furfural, NADPH and enzyme after 5 hours, (h) mass spectrum of furfuryl alcohol
497 standard. The full length GC traces can be found in figure S1.

498

499 Figure 2. MS analysis of the alcohol product from an incubation of 4-pyridine carboxaldehyde,
500 enzyme and either (A) NADPH or (B) (4R)-[4-(²H)]NADPD. The corresponding GC traces can
501 be seen in S2. (C) NMR spectra showing the purified nucleotide reaction product obtained from
502 incubations of Cbei_3974 with (4R)-[4-(²H)]NADPD and 4-pyridine carboxaldehyde (red)
503 against a standard of NADP⁺ (blue).

504 Figure 3. Kinetic isotope effects. Grey circles: k_{cat} values for natural abundance enzyme with
505 NADPH; blue circles: enzyme KIEs; red circles: substrate KIE (NADPH). All measurements
506 were made at 19 °C. Errors are standard deviations of three repeats.

507 Figure 4. The temperature dependency of the enzyme kinetic isotope effect (k_{cat} light enzyme /
508 k_{cat} heavy enzyme) with 3-pyridine carboxaldehyde as a substrate. Error bars show the standard
509 deviation of three repeats.

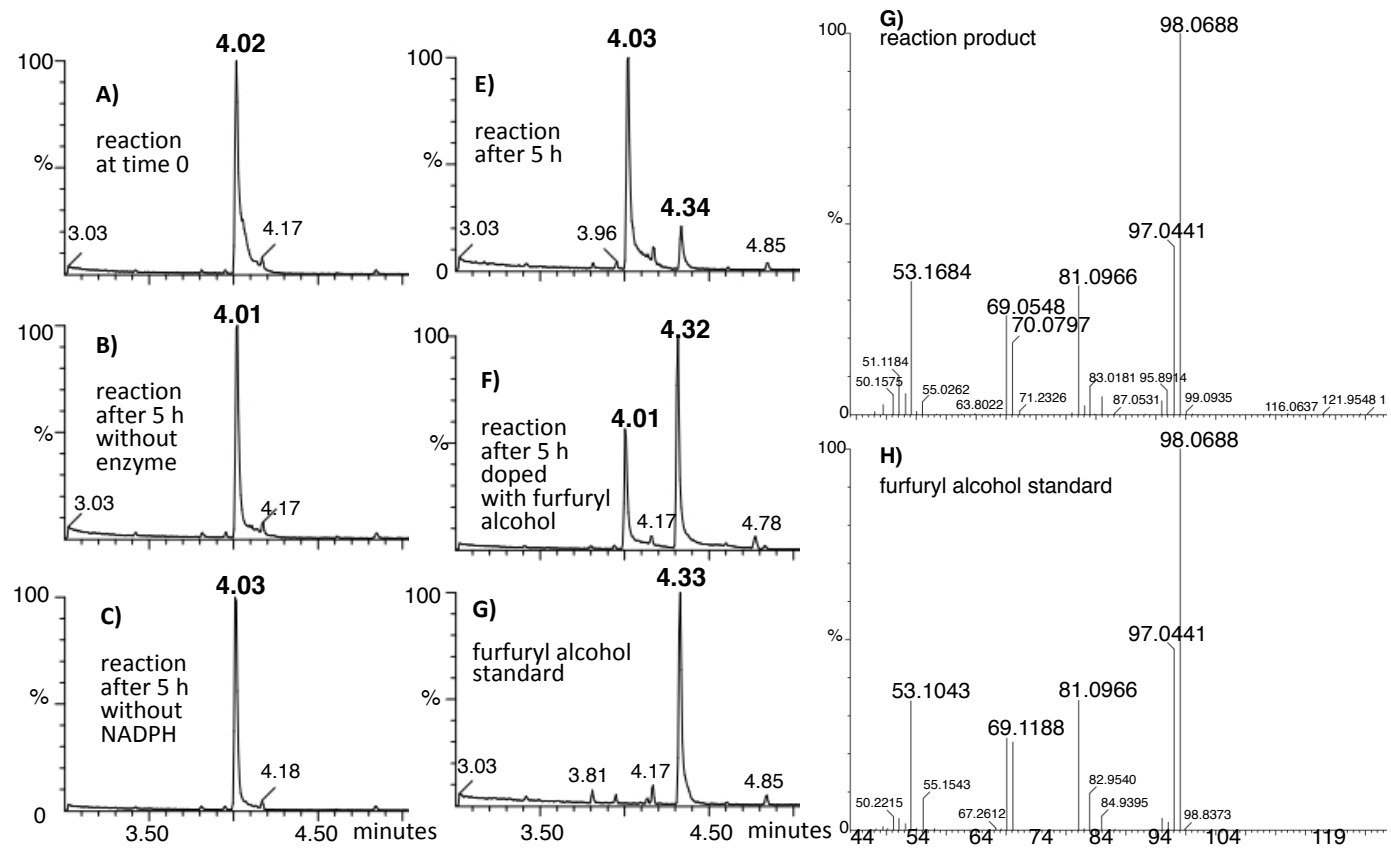
510 Figure 5. Crystal structure of Cbei_3974. **(A)** Cartoon representation showing the TIM barrel
511 fold. NADPH can be seen in gold, with the nicotinamide ring in the central cavity. **(B)** Surface
512 representation showing the exposed nature of the active site. NADPH shown in gold. **(C)**
513 Residues involved in binding NADPH. Red semicircles identify hydrophobic interactions,
514 residues involved in hydrogen bonds are shown in blue. The green numbers indicate hydrogen
515 bond distance. Figure prepared with LigPlot+ (22).

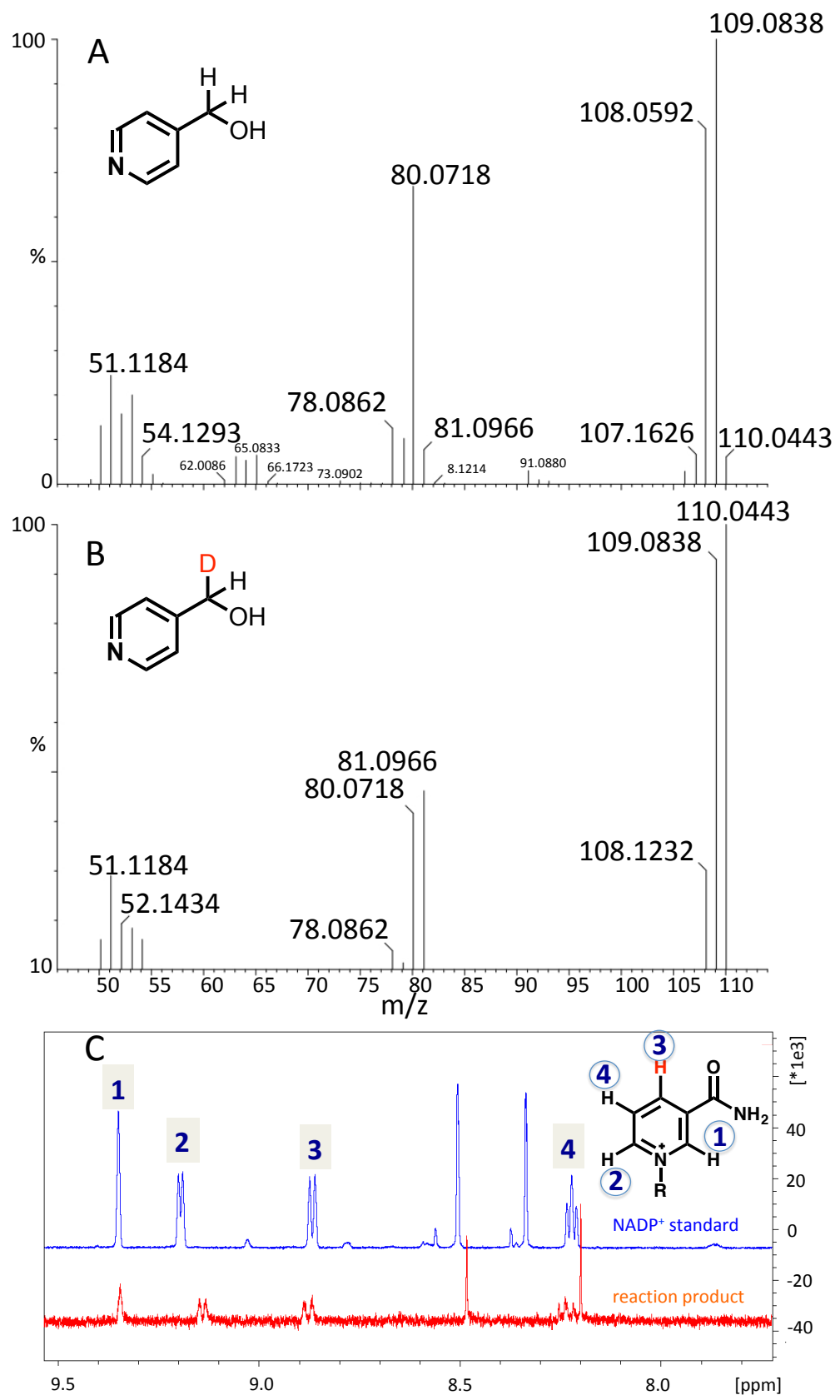
516 Figure 6. Docking of 4-pyridine carboxaldehyde **(A and B)** and furfural **(C and D)** into the
517 active site. Substrates are shown in orange. **(A and C)** show a hydrophobic surface rendering; **(B**
518 **and D)** identifies residues involved in binding (grey) and catalysis (green).

519

520

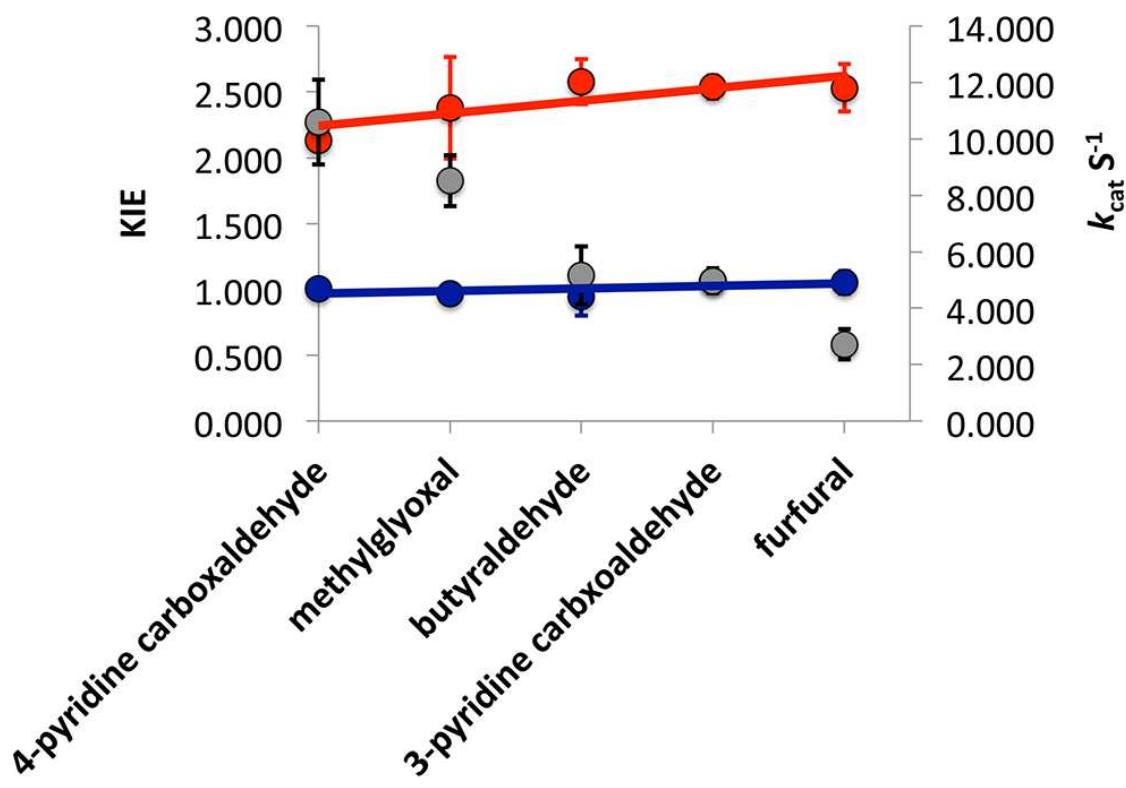
521





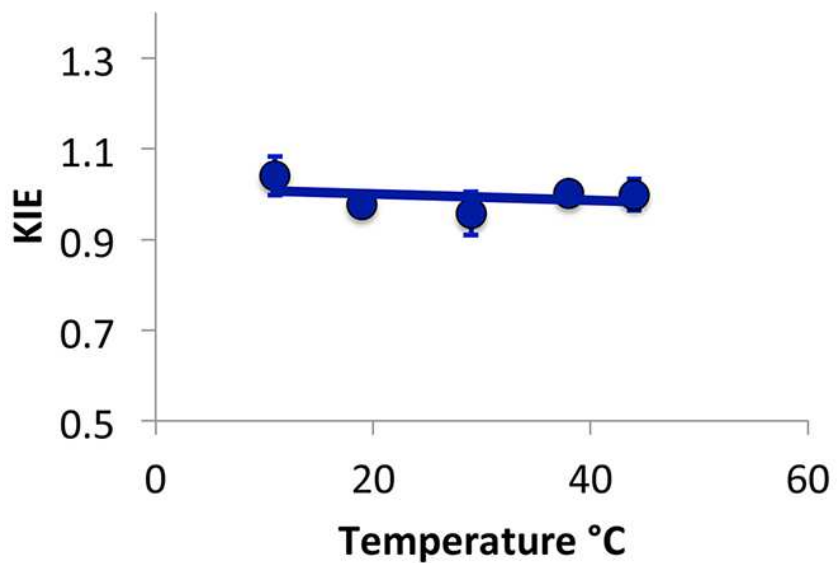
527

528



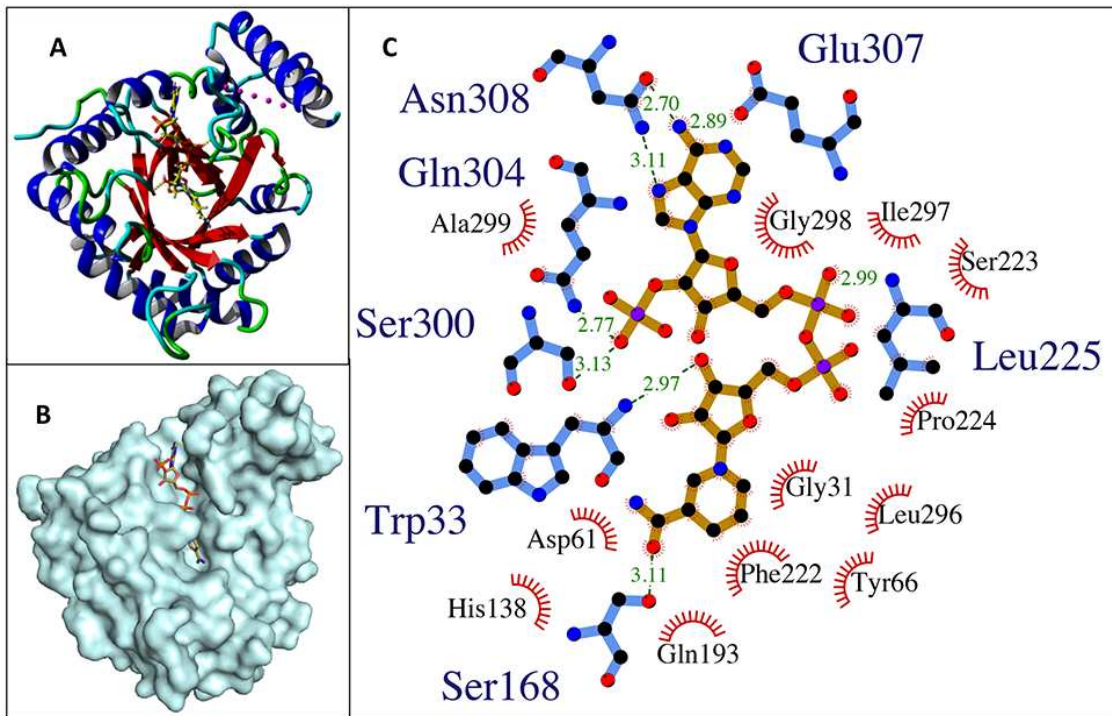
529

530



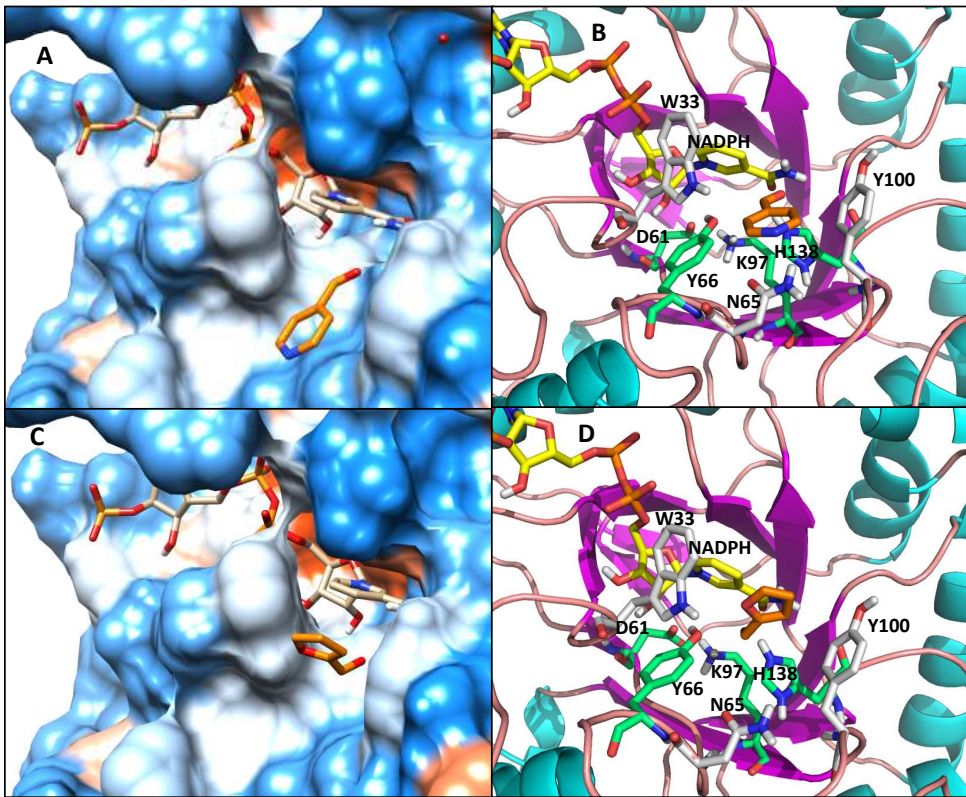
531

532



533

534



535

536